Torque Coordination of Clutch, Engine and Motor during Power Transition for a Hybrid Electric Bus

L. Chen, G. Xi, M.M. Zhang
National Key Lab of Automotive Electronics and Control, School of Mechanical Engineering
Shanghai Jiao Tong University, Shanghai, 200240, China
E-mail: li.h.chen@sjtu.edu.cn

***Abstract*-Ideal running performance requires that series-parallel hybrid electric vehicles smoothly transite between series and parallel operation modes. Clutches are widely applied to series-parallel hybrid electric vehicles to connect or disconnect powertrain components. Due to discontinuous nonlinear effect of clutch friction characteristics, smooth transition with little frictional dissipation is difficultly achieved. Hence, it is desirable to take friction discontinuity into consideration for improving the mode transition performance of hybrid electric vehicles. In this paper, a model reference adaptive control scheme based on hyperstability theory is developed to coordinate the torques of clutch, engine and motor for a post-transmission configured hybrid electric bus. It is worth emphasizing that the clutch is controlled to engage quickly and smoothly by a small frictional torque, which contributes directly to small jerk and little frictional dissipation. Results of simulations and experiments demonstrate that both vehicle jerk and frictional dissipation are decreased greatly compared to conventional operation. The effectiveness of the proposed adaptive control scheme is validated.**

I. INTRODUCTION

Series-Parallel Hybrid Electric Vehicles (SPHEVs) can improve efficiency and reduce emissions compared with standard electric vehicles because they can use both series and parallel energy management strategies. As a result, the vehicles can adapt to varied driving conditions. To obtain good performance, transitions between different operation modes of the SPHEVs must be executed smoothly.

In recent years, various mechanisms have been studied for coupling series and parallel power flows. These methods include planetary gears[1 , 2], continuous variable transmissions[3], switched powertrain with clutches[4,5,6]. Because of their high efficiency, small space requirements and structural evolution from conventional transmissions, clutches are widely used in novel coupler units of SPHEVs [7].

One configuration is the post-transmission SPHEV depicted in Fig. 1, in which an integrated starter and generator (ISG) as well as a traction motor (TM) is added to the powertrain. In motor-only driving mode, the clutch is disengaged, and the traction motor drives the vehicle solely using electricity from the battery. In parallel driving mode, the clutch is engaged, and the traction motor drives the vehicle together with the engine. The energy management strategy for this SPHEV has been estimated to reduce theoretical fuel consumption by up to 30.3% in Chinese transit buses[5]. However, numerous experiments have shown that the mode transition from motor-only to parallel driving may cause disturbances to the driver unless it is carefully controlled. The disturbances are like intensive jerk, overspeed engine and overwore friction of clutch plates. This has also been shown to be a serious problem in other hybrid vehicles with similar configurations[8].

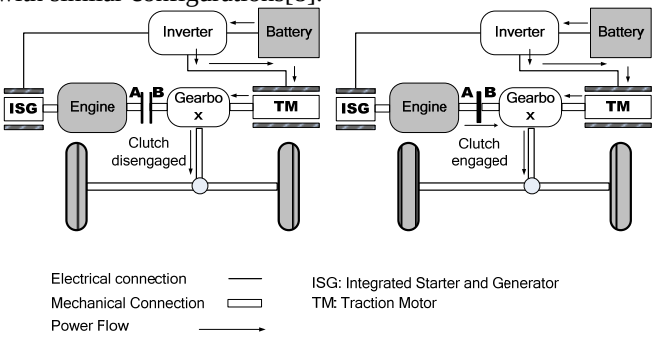

(a) motor-only driving mode (b) parallel driving mode

Fig. 1 Architecture of a SPHEV

To address the mode transition problem, a model predictive control approach has been applied to regulate torques of motors and a clutch[9]. A sub-domain controller based on state space partition was proposed for a class of switched hybrid dynamical systems. Simulation results show that clutch engagement characteristics are of major importance for increasing the smoothness in mode transitions. However, some of the existing solutions are based on heuristic techniques, and others do not explicitly express the clutch-involved modeling and control in the transitions.

Based on mathematical models considering nonlinear friction characteristics of the clutch, this paper proposes a model reference adaptive control(MRAC) in order to gain a smooth transition with little frictional dissipation for the SPHEV as shown in Fig. 1. In motor-only driving mode, the traction motor torque affects longitudinal dynamics of the vehicle. In parallel driving mode, the tranction motor torque together with the engine torque affect the vehicle dynamics. Therefore, function of the mode transition is to introduce the engine torque into the driveline by a controlled clutch torque. Since the mode transition should not disturb the vehicle dynamics, the vehicle is expected to run as if it were still in motor-only driving mode. From the control point of view, the three torques of the clutch, engine and traction motor should be coordinated to make the vehicle track its dynamics in the motor-only driving mode. This torque coordination is well suited for model reference adaptive control, which is a well-established method and has been used by many researchers [10,11,12]. In model reference adaptive control systems, the

978-1-4244-8218-4/10/$26.00 ©2010 IEEE

desired performance of the plant is expressed by a reference model that gives the desired response to a command signal. Hence, the designer is granted considerable flexibility in altering the goals by modifying the reference model. Thus, MRAC can overcome the challenges that other control algorithms experience because they have a predefined constant goal.

Under the MRAC architecture, a reference model is built to describe the desired driveline dynamics of the motor-only driving mode. The stability of MRAC is analysised based on Popov hyperstability theory[13]. The adaptive controller is regulated using state errors between actual dynamic states and referenced states. The MRAC method is applied to a SPHEV bus. The simulation and experimental results presented validate the effectiveness of MRAC and are compared with outcomes of a conventional control method.

II. DYNAMIC MODEL

The vehicle driveline that is involved in clutch engagement during the SPHEV mode transition can be treated as a multi-body system. For the purpose of simplification, the damping and elastic elements of the clutch that are used to reduce vibration and jerk are ignored, and all parts of the clutch assembly are assumed to exist in the form of concentrated masses[14]. The dynamic model is shown in Fig. 2, in which: J_1 is the total inertia moment of Shaft A including the crankshaft, flywheel, integrated starter and generator, and pressure plate of the clutch; J_2 is the total moment of inertia of Shaft B including the vehicle body, traction motor, gearbox and frictional plate of the clutch; ω_1 is the angular velocity of Shaft A, which is also the engine speed; ω_2 is the angular velocity of Shaft B, which is propotional to the vehicle speed; T_e is the driving torque applied to Shaft A, which is equal to the engine torque; T_c is the clutch frictional torque; T_{tm} is the tranction motor torque; and T_r is the resistant torque including the road, slope and wind resistance.

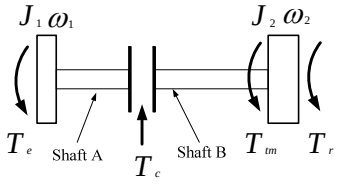

Fig. 2. Dynamic model of the SPHEV driveline

The generic dynamic equations in the mode transition of the SPHEV driveline can be written as:

$$J_1\dot{\omega}_1(t) = T_e - T_c \quad (1)$$

$$J_2\dot{\omega}_2(t) = T_{tm} + T_c + T_r \quad (2)$$

Equation (1) represents the dynamics of Shaft A, and equation (2) repsents that of Shaft B. The engine torque T_e can be expressed as a function of throttle opening α and the angular velocity $\omega_1(t)$ by $T_e = T_e(\alpha, \omega_1(t))$[14]. T_{tm} can be modeled as a function of $\omega_2(t)$, work load β and gear ratio i_{tm} from the traction motor to Shaft B by $T_{tm} = T_{tm}(\beta, \omega_2(t)) \cdot i_{tm}$ [5]. The resistance torque T_r can be expressed as a function of the vehicle mass m, road resistance coefficient f, angular velocity $\omega_2(t)$ of Shaft B, gear ratio i_1 of the gearbox, final drive ratio i_0 and tire radius R by $T_r = T_r(m, f, i_0, i_1, R, \omega_2(t))$[14].

When the friction plates of the clutch contact each other, denoted by $c = 1$, the classical Coulomb friction model is applied to T_c as shown in Fig. 3, where P_c is the normal pressure, μ is the slipping friction coefficient, and s is a constant relevant to geometry parameters of the clutch.

When $\omega_1 - \omega_2 \neq 0$, the friction is in slipping phase. In this phase, the direction of T_c depends on the angular velocity difference between ω_1 and ω_2, and the magnitude of T_c equals to the product of P_c, μ and s.

When $\omega_1 - \omega_2 = 0$, the friction is in sticking phase. In this phase, T_c is subject to a satuation, which equals to the product of P_c, μ and s. Its direction and magnitude vary along the dynamics of the whole drivetrain which employs the clutch.

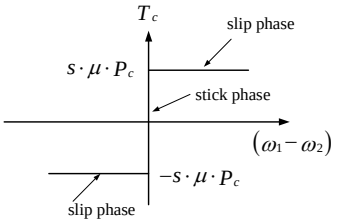

Fig. 3 Coulomb friction model

When the friction plates of the clutch do not contact each other, the clutch is in disengagement phase, denoted by $c = 0$. No friction torque is generated in this phase.

Typically, the clutch phase shifts from disengagement, to slipping and then sticking sequentially in the studied mode transition. It can be seen that T_c has segment expressions in the three phases, therefore, the dynamic equations (1) and (2) can be rewritten for each segment.

1) In the disengagement phase ($c = 0$)

In this phase, Shaft A and Shaft B are separated, and $T_c = 0$. Thus, T_e applies to Shaft A, T_{tm} applied to Shaft B, independently. The corresponding dynamic equations are rewritten as:

$$J_1\dot{\omega}_1(t) = T_e \quad (3)$$

$$J_2\dot{\omega}_2(t) = T_{tm} + T_r \quad (4)$$

2) In the slipping phase ($c = 1$ and $\omega_1 - \omega_2 \neq 0$)

In this phase, the dynamic equations are the same as in equations (1) and (2). According to Coulomb friction model, T_c has the following expression:

$$T_c = \text{abs}(\mu \cdot P_c \cdot R \cdot N) \cdot \text{sign}(\omega_1 - \omega_2) \quad (5)$$

in which abs(·) is the absolute value, sign(·) is the signum, and R is the equivalent acting radius of the frictional torque on the clutch plate, N is the number of frictional faces.

3) In the sticking phase ($c = 1$ and $\omega_1 - \omega_2 = 0$)

Combining equations (1) and (2) yields:

$$(J_1 + J_2)\dot{\omega}_2(t) = T_e + T_{tm} + T_r \quad (6)$$

The maximum value of T_c is limited by P_c as follows:

$$\text{abs}(T_c) \leq \text{abs}(\mu_s \cdot P_c \cdot R) \quad (7)$$

in which μ_s is the friction coefficient in the sticking phase.

T_c in the sticking phase is not an independent variable, and is decided by the other three torques from equations (1), (2) and (6).

$$T_c = \frac{J_2}{J_1+J_2}T_e - \frac{J_1}{J_1+J_2}T_{tm} - \frac{J_1}{J_1+J_2}T_r \quad (8)$$

The vehicle dynamics of the motor-only driving mode is treated as the reference model. The dynamic equation is:

$$J_2\dot{\omega}_2(t) = T_{tm} + T_r \quad (9)$$

III. MODEL REFERENCED ADAPTIVE CONTROLLER DESIGN

The Popov hyperstability theorem[13] is fundamental to stability analysis and the design of adaptive controllers for non-linear feedback systems. It has wide application potential compared with the unnecessarily complicated Lyapunov function. In the following sections, a MRAC model is designed based on the Popov hyperstability theorem for torque coordination during operation mode transition.

A. Popov Hyperstability Theorem

A feedback system is depicted in Fig. 4. The state equations of the linear system are as follows:

$$\dot{\boldsymbol{x}}(t) = \mathbf{A}\boldsymbol{x}(t) + \mathbf{B}\boldsymbol{u}(t) \quad (10)$$

$$\boldsymbol{y}(t) = \mathbf{C}\boldsymbol{x}(t) + \mathbf{D}\boldsymbol{u}(t) \quad (11)$$

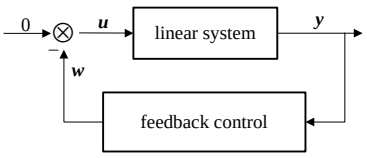

Fig. 4. Closed loop feedback system

where $\boldsymbol{x}$ is state vector, and $\boldsymbol{u}$ and $\boldsymbol{y}$ are the input and output vectors, respectively. $\mathbf{A}$, $\mathbf{B}$, $\mathbf{C}$ and $\mathbf{D}$ are constant matrices with corresponding dimensions. The pair $(\mathbf{A},\mathbf{B})$ is completely controllable, and $(\mathbf{A},\mathbf{C})$ is completely observable. Here, $\boldsymbol{y}$ and $\boldsymbol{w}$ are input and output of the feedback control block, respectively. The Popov integral inequality is defined as:

$$\int_{t_0}^{t_1} \boldsymbol{w}^T(t)\boldsymbol{y}(t)\,\mathrm{d}t \geq -r_0^2 \quad (12)$$

where $t_1 \geq t_0$, and r_0 is a positive constant which depends only on the initial state of the system and is independent of the integral upper limit t_1.

For the feedback control block that satisfies the inequalities in (12), the necessary and sufficient condition to guarantee the stability of the system in Fig. 4 is that the transfer function is positive real.

$$F(\mathrm{s}) = \mathbf{C}(\mathrm{s}\mathbf{I}-\mathbf{A})^{-1}\mathbf{B} + \mathbf{D} \quad (13)$$

in which s is the Laplace operator and $\mathbf{I}$ is a unit matrix.

The necessary and sufficient conditions for the real function $f(\mathrm{s})$ to be strictly positive real are:

1) real function $f(\mathrm{s})$ has no poles in the right half-plane $\mathrm{Re}(\mathrm{s}) > 0$ or on the $j\omega$ axis.

2) for any ω and $\mathrm{s} = j\omega$, the inequality $\mathrm{Re}\, f(j\omega) > 0$ exists.

B. MRAC Design

The following state variables are introduced:

$$x_{p1}(t) = \omega_1(t),\ x_{p2}(t) = \omega_2(t) \quad (14)$$

Suppose the inputs to the plant are:

$$u_1(t) = T_e,\ u_2(t) = T_{tm},\ u_3(t) = T_c,\ u_4(t) = T_r \quad (15)$$

The outputs of the plant are:

$$y_{p1}(t) = x_{p1}(t),\ y_{p2}(t) = x_{p2}(t) \quad (16)$$

The state equations are derived by using the dynamic equations for the three phases, respectively.

1) In the disengagement phase, there exists $u_3(t) = 0$. The state equations can be written as:

$$J_1\dot{x}_{p1}(t) = u_1(t) \quad (17)$$

$$J_2\dot{x}_{p2}(t) = u_2(t) + u_4(t) \quad (18)$$

The corresponding input-output equations are:

$$\dot{y}_{p1}(t) = \frac{u_1(t)}{J_1} \quad (19)$$

$$\dot{y}_{p2}(t) = \frac{u_2(t)+u_4(t)}{J_2} \quad (20)$$

2) In the slipping phase, the state equations can be written as:

$$J_1\dot{x}_{p1}(t) = u_1(t) - u_3(t) \quad (21)$$

$$J_2\dot{x}_{p2}(t) = u_2(t) + u_3(t) + u_4(t) \quad (22)$$

The corresponding input-output equations are:

$$\dot{y}_{p1}(t) = \frac{u_1(t)-u_3(t)}{J_1} \quad (23)$$

$$\dot{y}_{p2}(t) = \frac{u_2(t)+u_3(t)+u_4(t)}{J_2} \quad (24)$$

3) In the sticking phase, $u_3(t)$ is not an independent input because of the physics expressed in (8). The state equation can be written as:

$$(J_1+J_2)\dot{x}_{p2}(t) = u_1(t) + u_2(t) + u_4(t) \quad (25)$$

The input-output equations are:

$$\dot{y}_{p1}(t) = \dot{y}_{p2}(t) = \frac{u_1(t)+u_2(t)+u_4(t)}{J_1+J_2} \quad (26)$$

The input-output equations for the three phases can be summarized as:

$$\dot{y}_{pi}(t) = f_{pi}(u_1(t), u_2(t), u_3(t), u_4(t)) \quad i = 1,2 \quad (27)$$

According to the dynamic equation (9) of the reference model, assuming the state variable $x_m(t) = \omega_2(t)$, the state equation can be derived by:

$$J_2\dot{x}_m(t) = u_2(t) + u_4(t) \quad (28)$$

Assuming the output of the referenced model $y_m(t) = x_m(t)$, the input-output equation is:

$$\dot{y}_m(t) = \frac{u_2(t)+u_4(t)}{J_2} \quad (29)$$

The overall architecture of the MRAC system for this multi-input multi-output system is designed in Fig. 5. The flowcharts from w to v represent the linear system block from Fig. 4, including the reference model, the plant and a linear compensator $\mathbf{L}$. The adaptive regulator $\mathbf{K}$ represents the feedback controller block of Fig. 4. The linear compensator $\mathbf{L}$ and adaptive regulator $\mathbf{K}$ are designed in upcoming sections.

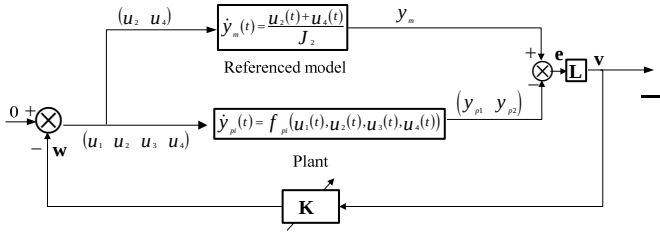

Fig. 5 Overall architecture of the model referenced adaptive control system

The flow chart for the coordinating algorithm is summarized in Fig. 6. Phase 1, Phase 2 and Phase 3 stand for the open phase, the slipping phase and the locked phase, respectively. ε is the threshold used to identify Phase 3. $h_{ij}(t)$ $(i=1,2 \quad j=1,2,3,4)$ and λ are control parameters.

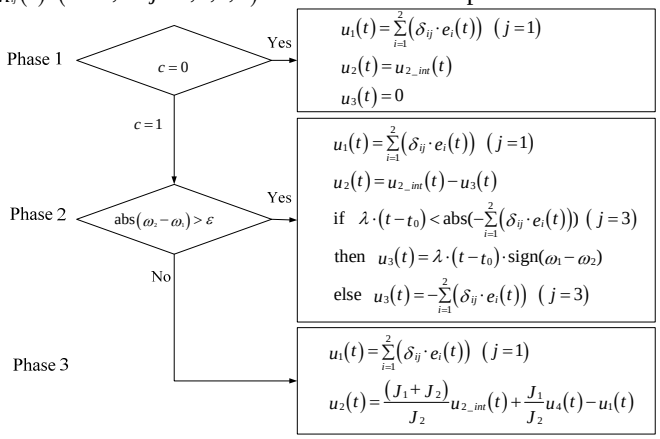

Fig. 6. Flowchart for torque coordination

IV. SIMULATION RESULTS

Many hybrid bus drivers have been observed pressing the accelerator pedal gradually and releasing the clutch pedal quickly during the power transition. They feel that operating in this way, named conventional operation, speeds the transition from the TM-driven mode to the engine-driven mode. The results of the conventional operation are used as a baseline against which the proposed MRAC results are compared.

The simulation takes SWB6116HEV as the prototype, with its parameters listed in Table 1.

TABLE 1. Parameters for simulation

Symbol	value
inertial moment of Shaft A J_1 ($kg \cdot m^2$)	1.8
vehicle mass m (kg)	16000
Inertial moment of traction motor J_{TM} ($kg \cdot m^2$)	0.88
Inertial moment of clutch frictional plate J_{clch} ($kg \cdot m^2$)	0.05
Inertial moment of final gear J_{fnl_gear} ($kg \cdot m^2$)	0.05
engine rated torque T_{e_max} (Nm)	550
traction motor peak torque T_{tm_max} (Nm)	450
final drive ratio i_0	5.571
first gear ratio i_1	3.78
gear ratio from traction motor to Shaft B i_{tm}	4
tire radius R (m)	0.525
coefficient of rolling resistance f	0.0015
number of frictional faces N	2
friction coefficient μ	0.42
equivalent acting radius of frictional torque R_c (m)	0.15

The clutch of SWB6116HEV is totally disengaged when the clutch pedal is pressed to the maximum position, and the clutch is gradually engaged when the clutch pedal is released after passing the clearance. The normal pressure P_c on the frictional plates is calculated by the following expression.

$$\begin{aligned} P_c &= 0 && (1\text{-}\alpha) \le \beta \le 1 \\ P_c &= b \cdot \left(1 - \frac{\beta}{1-\alpha}\right) && 0 < \beta \le (1\text{-}\alpha) \end{aligned} \tag{30}$$

where $\alpha(0 \le \alpha \le 1)$ is the clearance travel, $\beta(0 \le \beta \le 1)$ is the clutch pedal opening. For SWB6116HEV, α is 0.2, b is 15000N.

The control parameters of the MRAC algorithms in Fig.5 are $\lambda = 50$, $\delta_{11} = \delta_{21} = 1$, $\delta_{13} = \delta_{23} = 10$.

MRAC commands the torques according to the three phases of the clutch, which are designated in Fig.7(a). MRAC inceases the engine torque to reduce the speed difference between Shaft A and Shaft B in the open phase, then engages the clutch by releasing the pedal a little in the slipping phase, coordinating with a suitable engine torque till the clutch engaged, then releases the clutch pedel entirely and executes an engine torque control in the locked phase. The traction motor torque compensates the intervene from the engine torque and clutch torque to the dynamics of Shaft B, as shown in Fig. 7(b). The angular velocities of Shaft A and Shaft B are approaching gradually as shown in Fig.7(f).

Conventional operation increases the engine torque and releases the clutch pedal rapidly, thus, increases the clutch frictional torque quickly. It can be seen from Fig. 7(f) that the angular velocities of Shaft A and Shaft B synchronize in a short time.

For performance consideration, vehicle acceleration, vehicle jerk and frictional dissipation are evaluated. Vehicle jerk is calculated as the derivative of the vehicle acceleration[14]. Frictional dissipation is calculated using the following formula [14]:

$$F_D = \int_{t_1}^{t_2} \mathrm{abs}(\omega_1 - \omega_2) \cdot \mathrm{abs}(T_c)\, \mathrm{d}t \tag{31}$$

In the comparison in Fig. 7(g-i), big differences are shown between the two methods. The vehicle acceleration maintains when MRAC is applied, while falls down by around 2m/s2 when conventional operation is applied. This falling down shows a torque interruption of vehicle driveline. The reason lies that a big negative frictional torque is generated by the clutch, but no compensation is activated. For MRAC, the negative frictional torque is also generated by the clutch, but much smaller, and the traction motor increases its torque to compensate the negative effect, therefore, the torque interruption can be avoided.

The vehicle jerk from MRAC during the mode transition is less than $1\ \mathrm{m/s^3}$, while that from the conventional operation is up to $290\ \mathrm{m/s^3}$ which occurs at the end of the slipping phase. The reason for the sudden jerk is that the clutch

frictional torque changes suddenly because of a slip-stick friction transition at this point. In the slipping phase, the clutch frictional torque is basically proportional to the pressure. When the clutch entirely engages, the clutch enters the locked phase, and the clutch frictional torque is calculated by(8). The conventional operation releases the clutch pedal quickly in the slipping phase, leading to a large frictional torque at the end, which is much larger than that in the coming locked phase. Thereafter, an intensive jerk occurs when the clutch enters into the locked phase. For MRAC, the clutch frictional torque in the slipping phase is controlled to approach a referenced model, and the torque continuity is guarranted by the parameter calculation. So, MRAC avoids a sudden change of clutch torque in the slip-stick transition, and avoids the intensive vehicle jerk.

The frictional dissipation resulted from MRAC is 3300 J , while that from the conventional operation is up to 6400 J . The frictional dissipation is generated in the slipping phase. From expression (31), it is affected by three factors: the angular velocity difference, the frictional torque and the slipping duration. MRAC reduces the friction dissipation in two aspects. Firstly, the angular velocity difference is decreased by the engine torque control before the slipping phase. Secondly, MRAC produces a comparatively low frictional torque in the slipping phase, which can be seen in Fig.6(e). Although with MRAC the slipping duration is longer than with the conventional operation, the frictional dissipation is greatly reduced.

In summary, MRAC has much less vehicle torque interruption, vehicle jerk and frictional dissipation than the conventional operation. Thus, MRAC is advantageous for vehicle running performance and also for energy efficiency and clutch duration.

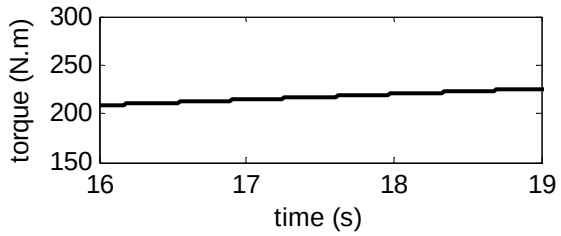

(a) Referenced torque for TM

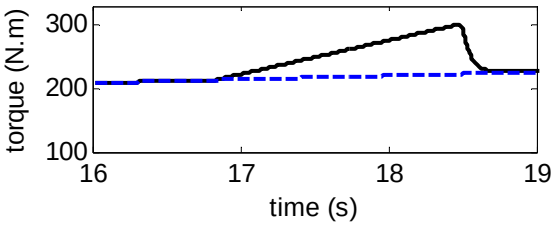

(b) TM output torque

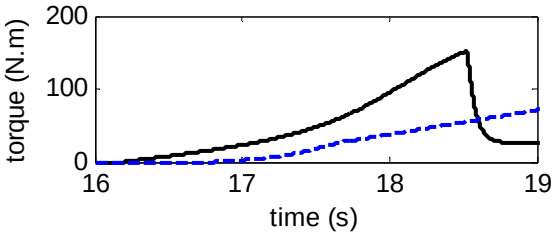

(c) Engine torque

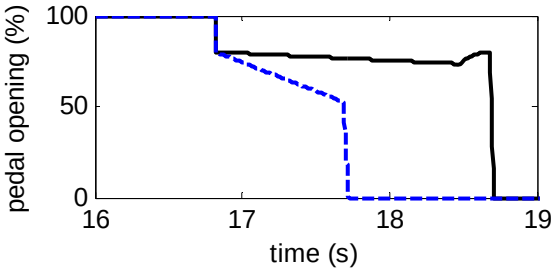

(d) Clutch pedal opening

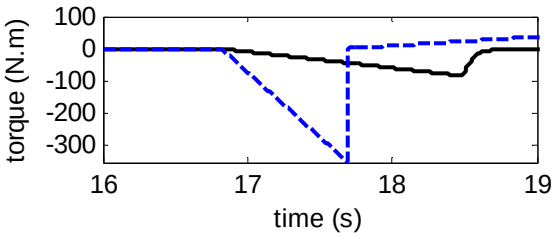

(e) Clutch frictional torque

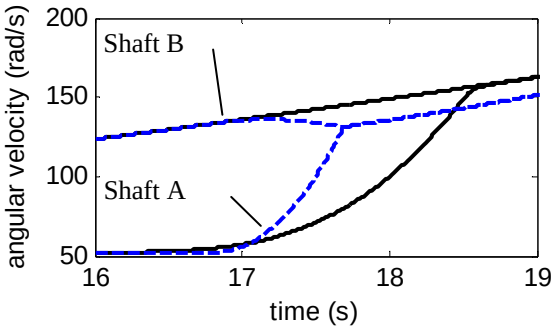

(f) Angular velocity

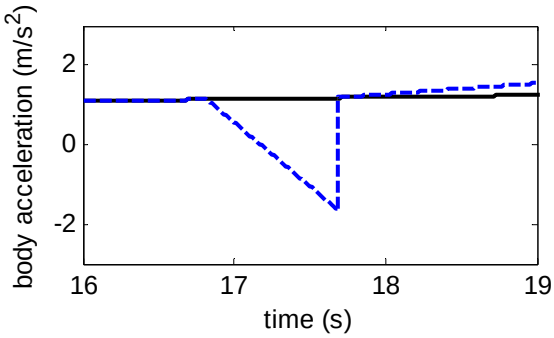

(g) vehicle acceleration

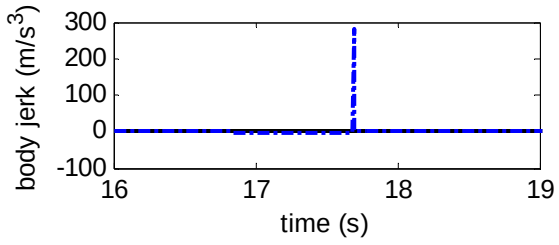

(h) Vehicle jerk

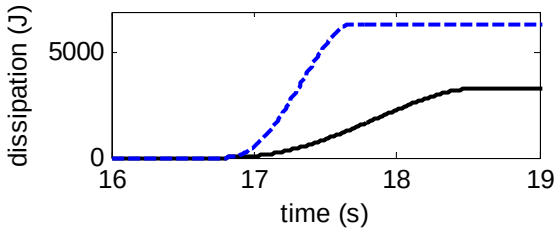

(i) Frictional dissipation

Fig. 7 Simulation results

V. CONCLUSION

The effects of friction-related nonlinearities and discontinuities of a SPHEV clutch on power transition dynamics were investigated. A model reference adaptive controller (MRAC) was proposed to compensate for the effects via torque coordination. Under the MRAC architecture, a reference model was built to describe the vehicle dynamics driven solely by a TM. A linear compensator and a regulator were derived using the Popov hyper-stability criterion.

In order to obtain acceptable levels of vehicle jerk and frictional dissipation during the clutch engagement stage of power transition, MRAC allowed the TM torque to keep up with the driver's intention, coordinating the engine torque to decrease the angular velocity difference between Shaft A and Shaft B before the clutch frictional torque was applied to the driveline. Unlike conventional operation where the frictional torque is increased rapidly at a constant rate, MRAC regulated the frictional torque along with the differences of the angular velocity and acceleration between the two shafts of the clutch. The frictional torque controlled by MRAC was very small, resulting in small vehicle jerk and small frictional dissipation. The simulation and experimental results show that MRAC can reduce both the vehicle jerk and frictional dissipation greatly as compared with conventional operation. So MRAC is advantageous for vehicle running performance and also for energy efficiency and clutch duration.

ACKNOWLEDGMENT

The authors would like to thank the Ministry of Science and Technology of the People's Republic of China as well as Shanghai Automotive Industry Co. Ltd. (SAIC) for their supports on this project (Grant No. 2006AA11A127).

REFERENCES

[1] J.M. Liu, H. Peng, Modeling and control of a power-split hybrid vehicle, IEEE transactions on Control Systems Technology 16 (6) (2008) 1242-1251

[2] J.Y. Park, Y.K. Park, J.H. Park, Optimal power distribution strategy for series–parallel hybrid electric vehicles, Proc. IMechE Part D: J. Automobile Engineering 222 (2008) 989-1000

[3] W. Ryu, N. Cho, I. Yoo, H. Song and H. Kim, Performance Analysis of a CVT Clutch System for a Hybrid Electric Vehicle, International Journal of Automotive Technology, 10(1)(2009) 115-121

[4] W. Lhomme, R. Trigui, P. Delarue, B. Jeanneret, Switched causal modeling of transmission with clutch in hybrid electric vehicles, IEEE Transactions on Vehicular Technology, 57 (4) (2008) 2081-2088

[5] W.W. Xiong, Y. Zhang, C.L. Yin, Optimal energy management for a series-parallel hybrid electric bus, Energy Conversion and Management, 50 (2009) 1730-1738

[6] B. Uli, R. Jörg, Hybridization possibilities of the dual clutch transmission, VDI Berichte 2030 (2008) 21-44

[7] M. Ehsani, Y.M. Gao, J.M. Miller, Hybrid electric vehicles: architecture and motor drives, Proceedings of the IEEE, 95 (4) (2007) 719-728

[8] K. Koprubasi, E. R. Westervelt, and G. Rizzoni, Toward the Systematic Design of Controllers for Smooth Hybrid Electric Vehicle Mode Changes, Proceedings of the 2007 American Control Conference, New York City, USA, (2007) 2985-2990

[9] R. Beck, S. Saenger, F. Richert, A. Bollig, K. Neiß_, T. Scholt_, K.-E. Noreikat_, D. Abel, Model Predictive Control of a Parallel Hybrid Vehicle Drivetrain, Proceedings of the 44th IEEE Conference on Decision and Control, and the European Control Conference, Seville, Spain, 2005 2670-2675

[10] L. Yacoubi, K. Al-Haddad, L.A. Dessaint, F. Fnaiech, Linear and nonlinear control techniques for a three-phase three-level NPC boost rectifier, IEEE Trans. Ind. Electron. 53 (6) (2006) 1908-1918

[11] K.K. Shyu, M.J. Yang, Y.M. Chen, and Y.F. Lin, Model reference adaptive control design for a shunt active-power-filter system, IEEE Transactions On Industrial Electronics 55 (1) (2008) 97-106

[12] Yung-Tien Liu, Kuo-Ming Chang,Wen-Zen Li, Model reference adaptive control for a piezo-positioning system, Precision Engineering 34 (2010) 62-69

[13] Popov VM, Hyperstability of control systems, New York: Springer-Verlag,1973.

[14] J.W. Zhang, L. Chen, G. Xi, System dynamic modelling and adaptive optimal control for automatic clutch engagement of vehicles，Proceedings of the Institute of Mechanical Engineers Part D: Journal of Automobile Engineerin 216 (2002) 983-991